creative commons

COMMONS DEED

저작자표시-비영리-변경금지 2.0 대한민국

이용자는 아래의 조건을 따르는 경우에 한하여 자유롭게

- 이 저작물을 복제, 배포, 전송, 전시, 공연 및 방송할 수 있습니다.

다음과 같은 조건을 따라야 합니다:

저작자표시. 귀하는 원저작자를 표시하여야 합니다.

비영리. 귀하는 이 저작물을 영리 목적으로 이용할 수 없습니다.

변경금지. 귀하는 이 저작물을 개작, 변형 또는 가공할 수 없습니다.

- 귀하는, 이 저작물의 재이용이나 배포의 경우, 이 저작물에 적용된 이용허락조건을 명확하게 나타내어야 합니다.
- 저작권자로부터 별도의 허가를 받으면 이러한 조건들은 적용되지 않습니다.

저작권법에 따른 이용자의 권리는 위의 내용에 의하여 영향을 받지 않습니다.

이것은 이용허락규약(Legal Code)을 이해하기 쉽게 요약한 것입니다.

Disclaimer

dCollection

[UCI]I804:48009-200000285822

理學碩士 學位 論文

Rational Synthesis of MoS_2-Cu_2O Hierarchical Photocatalysts for Efficient Visible-Light-Driven Photodegradation of Pollutants

(오염물질의 가시광을 통한 효율적인 광분해를 위한 이황화몰리브덴-산화구리(I) 광촉매의 합성)

蔚 山 大 學 校 大 學 院

化 學 科

劉 恩 辰

Rational Synthesis of MoS_2-Cu_2O Hierarchical Photocatalysts for Efficient Visible-Light-Driven Photodegradation of Pollutants

指 導 敎 授 홍 종 욱

이 論文을 理學碩士 學位 論文으로 제출함

2020年 2月

蔚 山 大 學 校 大 學 院

化 學 科

劉 恩 辰

劉 恩 辰의 理學碩士 學位 論文을 認准함

審査委員 이 민 형 印

審査委員 홍 종 욱 印

審査委員 하 지 원 印

蔚 山 大 學 校 大 學 院

2020年 2月

국문요약

지난 10년 동안 수중 유기 오염 물질을 제거하기 위해 반도체 물질을 광촉매로 사용하는 것이 점차 일반화되었고, 폐수에 함유된 의약품 및 개인위생용품 (PPCP)의 효과적인 처리는 환경 복원을 위한 중요 과제로 남아 있습니다. 현재 태양 에너지는 태양 전지, 광전기를 이용한 물 분해, 광촉매를 이용한 수소 생성 및 CO_2 광환원 및 광촉매를 이용한 오염물질의 분해에 크게 이용되어왔습니다. 그중 광촉매를 통한 화학 물질로부터 태양 에너지로의 전환은 현재 직면하고 있는 에너지 및 환경 문제를 해결하는 데 큰 도움이 됩니다. 지금까지 TiO_2는 UV 조사 하에서 폐수에 함유된 PPCP 및 유기 오염물질의 처리를 위한 가장 일반적인 광촉매로서 등장했습니다. 그러나 표면적이 작고 가시광선에 대한 광 활성이 없기 때문에 태양광에서 효율이 제한적입니다. 따라서, 가시광 조사 하에서 PPCP 및 유기 오염물질을 처리하기 위한 효율적인 광촉매의 개발이 필요합니다.

다양한 금속 산화물 중에서, 독특한 광학 및 전기적 특성을 갖는 잘 알려진 p형 반도체 물질인 산화 제1 구리 (Cu_2O)는 태양 에너지 변환, 센서, 광촉매 분해 및 여기자의 응집 전파에 대해 각광받는 물질입니다. 또한 Cu_2O의 밴드 갭 에너지인 2.0 eV는 넓은 밴드 갭 반도체에 비해 햇빛을 최대한 활용하는 데 큰 이점이 있습니다. 따라서, 가시광선 조사 하에서 물 분해 및 유기 오염 물질의 분해를 위한 Cu_2O 나노 결정의 제조가 널리 연구되어왔습니다. 그러나 이러한 이점에도 불구하고, 실제 적용은 낮은 광 수확 효율, 빠른 전하 재결합 및 광촉매의 낮은 안정성으로 인해 제한됩니다. 이황화 몰리브덴 (MoS_2)과 같은 2 차원 반도체는 전자, 광전자 및 에너지 수확에 광범위하게 적용할 수 있는 물질 군으로 부상하고 있습니다. MoS_2는 나노 기술에 사용될 수 있는 유망한 물질 중 하나이며 몇 개의 원자 층으로 만들어질 수 있습니다. 소수의 원자 층으로 구성된 MoS_2 나노 시트는 표면적이 넓기 때문에 가시광선 영역에서 광촉매 및 광전지 효율이 향상됩니다.

본 연구에서는 유기 오염 물질의 제거를 위해 효율적인 태양 에너지 수확 플랫폼인 Cu_2O-MoS_2를 개발했습니다. Cu_2O-MoS_2 나노 복합체는 Cu_2O를

MoS_2 나노 시트 상에 성장시켜 제조하였습니다. 반도체 광촉매의 제조는 특정 결정면으로 구성되며 광촉매의 오염 물질 분해 성능을 향상시키는 유망한 접근법 중 하나입니다. 비등방성 광촉매는 노출된 두 반도체 표면이 효과적으로 전하를 전달하여 지속적인 전하 균형을 이끌 수 있으므로 광촉매 활성을 향상시키기 위해 바람직합니다. 따라서 태양광을 이용한 광촉매로써 효과적인 Cu_2O와 MoS_2 나노 시트를 이용하여 다양한 모양의 비등방성 광촉매를 합성하여 유기 염료 및 제약 제품의 분해 능력을 알아보았습니다. 샘플은 X선 회절법, 주사 전자 현미경, 투과 전자 현미경 및 UV-Vis 분광기를 통해 특성을 확인하였습니다. 또한 전자스핀공명 분석, UV-Vis 확산 반사율 분석 그리고 전자-정공 스캐빈저 실험을 통해 광촉매 분해 매커니즘을 알아보았습니다. MoS_2 나노 시트에 성장한 Cu_2O 큐브 나노 입자의 크기는 약 28-33 nm입니다.

각각의 합성된 촉매로 가시광 조사 하에서 테오필린(theophylline) 및 메틸 오렌지(methyl orange) 제거에 의한 광촉매 활성 실험을 수행하였습니다. Cu_2O_{cube}-MoS_2 나노 복합체는 순수한 Cu_2O 나노 입자 및 MoS_2, Cu_2O_{octa}-MoS_2, CuO_{needle}-MoS_2 그리고 Cu_2O_{sphere}-MoS_2와 비교하여 크게 향상된 광촉매 효율을 보여주었습니다. Cu_2O_{cube}-MoS_2의 향상된 광촉매 성능은 주로 태양 에너지 흡수 효율뿐만 아니라 Cu_2O에서 MoS_2 나노 시트로의 효율적인 전하 수송 및 분리에 기인합니다.

결론적으로, 간단한 합성 방법을 통하여 MoS_2 나노 시트에 여러 광촉매를 성장시킨 나노구조체를 합성하였고, 이를 이용하여 물속에 존재하는 오염물질의 광촉매 분해 효율을 알아보았습니다. 그 결과 Cu_2O_{cube}-MoS_2는 가시광 ($\lambda \geq 400$ nm) 조사하에서 테오필린 및 메틸 오렌지의 광촉매 분해에 대하여 순수한 나노 입자, 다른 모양의 Cu_2O와 CuO 물질보다 우수한 활성을 나타내었습니다. 이는 복합 구조로 인해 증가된 광 흡수량 및 광 생성된 전자-정공 쌍의 효율적인 분리뿐만 아니라 증가된 표면적의 상승효과에 기인할 수 있습니다. 이 연구는 환경 보호뿐만 아니라 오염된 폐수를 분해하기 위한 잠재적인 산업 응용 분야에 적용을 위한 가시광선 광촉매의 제조와 개발에 대한 간단한 전략을 제공할 수 있을 것으로 기대됩니다.

Abstract

The use of semiconductors as photocatalysts to remove organic pollutants in water over the past decade has become increasingly common, and effective treatment of pharmaceuticals and personal care products (PPCP) in wastewater remains an important challenge for environmental restoration. Currently, solar energy has been wildly utilized for solar cell, photoelectrochemical water splitting, photocatalytic hydrogen production and CO_2 photoreduction, and photocatalytic degradation of pollutants. Among them, the conversion of chemicals into solar energy through photocatalysts is a big part of solving the current energy and environmental challenges. To date, TiO_2 has emerged as the most common photocatalyst for the treatment of PPCP and organic pollutants contained in wastewater under UV irradiation. However, the efficiency is limited in sunlight due to the small surface area and lack of light activity for visible light. Therefore, there is a need for the development of efficient photocatalysts for the treatment of PPCP and organic contaminants under visible light irradiation.

Among various metal oxides, cuprous oxide (Cu_2O), a well-known p-type semiconductor material with unique optical and electrical properties, is an appealing candidate for solar energy conversion, sensors, photocatalytic degradation and coherent propagation of excitons. In addition, Cu_2O with band gap energy of 2.0 eV has a significant advantage in making the most of sunlight compared to wide band gap semiconductors. Therefore, the preparation of Cu_2O nanocrystals for water decomposition and decomposition of organic pollutants under visible light irradiation has been widely studied. However, despite these advantages, practical applications are limited to low light harvesting efficiency, fast charge recombination and low stability of photocatalysts. Two-dimensional semiconductors such as molybdenum disulfide (MoS_2) are emerging material family with wide-ranging potential applications in electronics, optoelectronics and energy harvesting. MoS_2 is one of the promising materials that can be used in nanotechnology and it can be made as a few atomic layers. MoS_2 nanosheets composed of a few atomic layers have high surface area, which improves photocatalytic and photovoltaic efficiency in visible light region.

In this study, we developed Cu_2O-MoS_2, an efficient solar energy harvesting platform for the removal of organic contaminants. Cu_2O-MoS_2 nanocomposites were prepared by growing Cu_2O on MoS_2 nanosheets. The fabrication of semiconductor photocatalysts consists of

specific facet and is one of the promising approaches to improve the photocatalytic decomposition efficiency of contaminants. Anisotropic photocatalysts are desirable to enhance photocatalytic activity because the two exposed semiconductor surfaces can effectively carry charge and lead to a constant charge balance. Therefore, we analyzed the decomposition ability of organic dyes and pharmaceutical products by synthesizing anisotropic photocatalysts of various shapes using Cu_2O and MoS_2 nanosheets, which are effective as photocatalysts using sunlight. Samples were characterized by X-ray diffraction, scanning electron microscopy, transmission electron microscopy, and UV-Vis spectrophotometry. The photocatalytic decomposition mechanism was also investigated through electron spin resonance analysis, UV-Vis diffuse reflectance analysis, and electron-hole scavenger experiments. The size of Cu_2O cube nanoparticles grown on MoS_2 nanosheets is about 28-33 nm.

Each synthesized catalyst was tested for photocatalytic activity by removing theophylline and methyl orange under visible light irradiation. Cu_2O_{cube}-MoS_2 nanocomposites showed significantly improved photocatalytic efficiency compared to pure Cu_2O nanoparticles and MoS_2, Cu_2O_{octa}-MoS_2, CuO_{needle}-MoS_2 and Cu_2O_{sphere}-MoS_2. The improved photocatalytic performance of Cu_2O_{cube}-MoS_2 is mainly ascribed to enhanced efficiency for solar energy absorption as well as the efficient charge transportation and separation from Cu_2O to MoS_2 nanosheets.

In conclusion, we have synthesized nanostructures in which several photocatalysts were grown on MoS_2 nanosheets by simple synthesis method, and we investigated the photocatalytic decomposition efficiency of pollutants in water. As a result, Cu_2O_{cube}-MoS_2 displayed enhanced activity than pure nanoparticles, different shapes of Cu_2O and CuO materials, for photocatalytic degradation of theophylline and methyl orange under visible light ($\lambda \geq 400$ nm) irradiation. This can be attributed to the synergistic effect of the increased light absorption intensity and efficient separation of the photo-generating electron-hole pairs as well as the increased surface area due to the complex structure. This research is expected to provide a simple strategy for the manufacture and development of photocatalysts using visible light for application not only for environmental protection but also for potential industrial applications for the decomposition of contaminated wastewater.

Index

Korean abstract ····· i

Abstract ····· iii

I. Introduction ····· 1

II. Experimental Section ····· 4

III. Result and Discussion ····· 6

III-1. Characterizations ····· 6

III-2. Photocatalytic Property and Mechanisms ····· 21

IV. Conclusion ····· 33

V. Reference ····· 34

I. Introduction

Effective remediation technologies to eliminate pollutants with detrimental environmental effects have been recognized as a hot issue for preventing destruction of environment.[1-3] Among various pollutants in wastewater, in particular removal treatments for organic dyes and pharmaceutical products have attracted enormous attention due to its high toxicity, widespread usage, difficulty for complete elimination via ordinary removal approach.[4-6] Although recently developed strategies have been applied to diminish organic dyes and pharmaceutical products included in wastewater,[7-12] second types of pollutants were generated by incomplete degradation and insufficient removal efficiency, which demands the development of innovative approach to effectively convert pollutants into non-hazardous molecules.[13] In this regard, among various techniques, photocatalytic wastewater treatment by using nanocatalysts is a one of the most promising approaches, where the design of nanocatalysts is one of the most important factors for effective photocatalytic efficiency. Nanostructures used as photocatalysts for photocatalytic wastewater treatment should efficiently harvest solar energy to generate high density of charge carriers, which can lead rapid degradation of pollutants. During the past decades, myriad metal oxide and chalcogenide photocatalysts have developed and showed positive potential in various photocatalytic reactions including conversion of a wide range of pollutants to non-hazardous molecules. However, such single semiconductors have some limitations such as narrow optical window, rapid recombination of electrons and holes, low charge mobility, and low stability.

To overcome the drawbacks of single semiconductor photocatalysts, binary semiconductor-semiconductor heteronanocrystals (HNCs) composed of hetero-junction between two different semiconductors with complementary band gap, desirable CB/VB potentials is one of desirable photocatalysts. Binary photocatalysts can not only promote formation and migration of charge carriers, but also suppress the recombination of photo-induced charge carriers, boosting solar energy conversion efficiency.[14,15] In this regard, it is worth noting that charge equilibrium in binary photocatalysts by continuous consumption of charge carriers is a prerequisite for exploiting the above benefits. Indeed, various binary core-shell and ill-regular shaped photocatalysts constructed with only one type of semiconductor surface showed underperforming photocatalytic activities due to inefficient charge equilibrium. In contrast, anisotropic binary photocatalysts composed of two exposed semiconductors remarkably

improved photocatalytic activities, because photo-induced charge carriers can readily react with reactive molecules through both exposed semiconductor surfaces, which can lead the sustainable charge equilibrium. Therefore, anisotropic binary photocatalysts are highly desirable for enhancement of photocatalytic activity. On the other hand, preparation of semiconductor photocatalysts consist of particular facets has also emerged as one of promising approaches for improving photocatalytic performance. Distinct from semiconductor photocatalysts with random-facets due to their ill-regular shapes, shape-controlled photocatalysts are enclosed of particular facets, which can promote photocatalytic activity.[16-18] Given that binary photocatalysts constructed with semiconductors of complementary band gaps, desirable CB/VB potentials, and optimal facets obtained by shape control are highly effective for boosting photocatalytic efficiency, HNCs produced by growing the shape-controlled semiconductor nanocrystals (NCs) with particular facets on pre-synthesized semiconductor nanostructures is able to effectively improve the photocatalytic pollutant degradation performance. However, owing to huge difficulties in simultaneously achieving both the shape-control and anisotropic morphology of semiconductor nanostructures via coupling of two semiconductors with intimate connection, the realization of such anisotropic binary photocatalysts is a highly challenging work and has scarcely been reported, although a few binary HNCs composed of un-controlled shapes was reported.

Of various combinations of semiconductor-semiconductor, Cu_2O-MoS_2 combination is intriguing candidate as a photocatalyst. Cu_2O has direct band gap of 2.0 eV-2.2 eV,[19,20] which can effectively facilitate the absorption of visible-light. In addition,_negative position of conduction band (CB) edge potential of Cu_2O than LUMO of oxygen ionosorption, which is process for production of O_2-·(ads) by reduction of O_2, can expedite photocatalytic pollutant degradation via indirect pathway. On the other hand, Cu_2O-MoS_2 binary photocatalysts also lead the efficient absorption of a wide range of light due to complementary band gaps of MoS_2 (1.2–1.8 eV)[21] and Cu_2O (2.0 eV). Moreover, owing to distinct band edge potentials of MoS_2 and Cu_2O, Cu_2O-MoS_2 binary photocatalysts can effectively promote the migration of photo-induced electrons and holes to each opposite semiconductor surfaces, and thus lead retardation of recombination of charge carriers.

In this work, we present novel synthetic strategy for anisotropic Cu_2O NC-MoS_2 HNCs such as Cu_2O nanocube-MoS_2 (Cu_2O_{cube}-MoS_2) and Cu_2O nanooctahedron-MoS_2 (Cu_2O_{octa}-MoS_2)

HNCs prepared through shape-controlled growth of Cu_2O nanocubes and nanooctahedra on chemically exfoliated MoS_2 (ce-MoS_2) nanosheets, respectively. Since anisotropic Cu_2O_{cube}-MoS_2 and Cu_2O_{octa}-MoS_2 HNCs are composed of {100}- and {111}-bounded Cu_2O surfaces, respectively, they can be used as an effective platform for investigating the effects of semiconductor surfaces and anisotropic morphologies on photocatalytic performance. Therefore, the investigation with anisotropic binary HNCs with different surface structures will allow developing efficient photocatalysts for pollutant degradation. Indeed, the present work demonstrates that the photocatalytic performances of Cu_2O-MoS_2 HNCs highly depend on both the facet of Cu_2O NCs and coupling of Cu_2O and MoS_2. We found that Cu_2O_{cube}-MoS_2 HNCs enable excellent photocatalytic activities toward degradation of methyl orange (MO) and theophylline under visible-light due to synergistic compositional and structural benefits.

II. Experimental Section

Chemicals and materials. Copper(II) chloride ($CuCl_2$, 99.999%, Sigma-Aldrich), sodium dodecyl sulfate (SDS, ≥99.0%, Sigma-Aldrich), hydroxylamine hydrochloride ($NH_2OH{\cdot}HCl$, 98.0%, Sigma-Aldrich), sodium hydroxide beads (NaOH, 97%, DAEJUNG), hydrazine monohydrate (N_2H_4, 64-65 %, Sigma-Aldrich), citric acid (99%, pure, anhydrous, Acros Organics), molybdenum(IV) sulfide (MoS_2, Sigma-Aldrich), and *n*-butyllithium solution (2.5 M in hexanes, Sigma-Aldrich) were used as received. Ultrapure distilled and deionized water (18.2 MΩ) was used for all solution preparations.

Preparation of ce-MoS_2. In a typical preparation of ce-MoS_2, 4 mL of n-butyllithium solution (2.5 M in hexanes) were added to 0.5 g of bulk MoS_2 and the resultant mixture were left in room temperature for 2 days. After 2 days, the mixture was sonicated for 2 h and centrifuged at 5000 and 10000 rpm respectively.

Preparation of Cu_2O nanooctahedra. For the synthesis of Cu_2O octahedron, 1 mL of NaOH (0.35 M) solution is quickly added to 30 mL of $CuCl_2$ (0.0032 M) aqueous solution under constant strong stirring. Then 78.5 μL of N_2H_4 (13.4 M) is quickly dropped in the above solution at room temperature. The precipitates were quickly collected through centrifugation (5000 rpm for 5 min) and washed three times with distilled water and ethanol respectively.

Preparation of Cu_2O nanocubes. For the synthesis of Cu_2O nanocubes, 0.5 mL of $CuCl_2$ (0.1 M) and 3 mL of SDS (0.1 M) were added in 8.92 mL of deionized water in a water bath set at 32–34 °C. Then 0.18 mL of NaOH (1.0 M) solution was introduced. Finally, 0.5 mL of $NH_2OH{\cdot}HCl$ (0.1 M) were quickly injected in 5 s with constant stirring. The solution were kept in the water bath for 30 min for nanocrystal growth and centrifuged at 5000 rpm for 5 min. The precipitate was washed with 5 mL of ethanol. The precipitate was centrifuged and washed again using ethanol to remove unreacted chemicals and SDS surfactant.

Preparation of Cu_2O octahedra on MoS_2 sheets. In the first step, 1 mL of an aqueous solution of ce-MoS_2 (1.52 mM) and 1 mL of citric acid (0.095 mM) were added into a 5.92 mL of deionized water in a water bath set at 40 °C with constant stirring. After 1 h, 200 μL of $CuCl_2$ (100 mM) were introduced and 0.208 mL of NaOH (0.35 M) solution is quickly added under constant strong stirring. Then 10 μL of N_2H_4 (13.4 M) is quickly dropped in the above

solution at room temperature. The solution were quickly centrifuged at 8000 rpm for 5 min. The final product was washed two times with deionized water and ethanol.

Preparation of Cu_2O cubes on MoS_2 sheets. In the first step, 1 mL of an aqueous solution of ce-MoS_2 (1.52 mM) and 1 mL of citric acid (0.095 mM) were added into a 5.92 mL of deionized water in a water bath set at 40 °C with constant stirring. After 1 h, 1.8 mL of SDS (100 mM) and 200 μL of $CuCl_2$ (100 mM) were introduced. Then aged for 1 h in 32 °C water bath. Finally, 72 μL of NaOH (1.0 M) was introduced first and 200 μL of $NH_2OH{\cdot}HCl$ (100 mM) were quickly injected in 5 s. The solution were kept in the water bath for 1 h for nanocubes growth and centrifuged at 8000 rpm for 5 min. The final product was washed two times with deionized water and ethanol.

Preparation of different shape of heterostructure catalysts. For the synthesis of CuO_{needle}/MoS_2 catalysts, 144 μL of NaOH (1.0 M) and 200 μL of $NH_2OH{\cdot}HCl$ (100 mM) were added in the final step of Cu_2O cube/MoS_2 synthesis. For the synthesis of Cu_2O_{sphere}/MoS_2 catalysts, 72 μL of NaOH and 400 μL of $NH_2OH{\cdot}HCl$ were added in the final step of Cu_2O cube/MoS_2 synthesis.

Characterizations of the samples. Transmission electron microscopy (TEM) and scanning electron microscopy (SEM) images of the synthesized nanocrystals were obtained on Jeol JEM-2100F and Jeol JSM-7610F, respectively. X-ray diffraction (XRD) measurement were conducted on a Bruker D8 Advance scanning for 2 θ at 10 to 80 degree. X-ray photoelectron spectroscopy (XPS) measurements were conducted on a ThermoFisher K-alpha.

Photocatalysis Experiments. For the photocatalytic activity measurements, 2.5 mg reagent amount of photocatalysts was dispersed into a 20 mL aqueous solution containing 1 mg of theophylline and 1 mg of methyl orange, and the resultant solution was transferred to a quartz cell. The cell was irradiated with visible-light by using a 300 W Xe lamp (Newport 66902) equipped with a UV-cutoff filter (>400 nm). The intensity of light at the cell was measured to be 70.37 mW/cm^2.

III. Result and Discussion

III-1. Characterizations

The synthetic procedure for Cu_2O NC-MoS_2 HNCs is illustrated in Figure 1a. The ce-MoS_2 nanosheets were first prepared by chemically exfoliation method from bulk MoS_2. The scanning electron microscopy (SEM) and transmission electron microscopy (TEM) images showed that thin 2D nanosheets are successfully prepared (Figure 1b-c), which are used as 2D template for Cu_2O NC-MoS_2 HNCs. The high-resolution TEM (HRTEM) image of the ce-MoS_2 nanosheet and corresponding the fast Fourier transfer (FFT) pattern (inset of Figure 1c), displaying low crystallinity of ce-MoS_2 nanosheet. This was further investigated by using X-ray diffraction (XRD) measurement. The atomic force microscopy (AFM) image and line profile of ce-MoS_2 nanosheets were obtained to investigate its thickness, indicating that the average thickness of ce-MoS_2 nanosheets was 0.95 nm (Figure 1d). To prepare the Cu_2O_{cube}-MoS_2 HNCs, Cu_2O nanocubes were directly formed on ce-MoS_2 nanosheets by using NaOH and NH_2OH•HCl in an aqueous solution including sodium dodecyl sulfate (SDS). Figure 1e and Figure 1f showed SEM and TEM images of obtained Cu_2O_{cube}-MoS_2 HNCs, respectively, showing the formation of uniform nanocubes on the 2D ce-MoS_2 nanosheets. The average edge length of nanocubes was determined as 28 ± 33 nm. The d-spacing for adjacent lattice fringes in the high-resolution TEM (HRTEM) images of a nanocube formed on ce-MoS_2 nanosheets is 0.23 nm (inset of Figure 1f), which corresponds with that of {100} plane of Cu_2O. The FFT pattern obtained from a nanocube along [001] zone axis indicates its single crystalline (inset of Figure 1f).[22,23]

The Cu_2O_{octa}-MoS_2 HNCs were prepared by growing the Cu_2O nanooctahedra on ce-MoS_2 sheets by using hydrazine as a reducing agent instead of NH_2OH•HCl while other synthetic condition for Cu_2O_{cube}-MoS_2 HNCs were unchanged (Figure 1a). Typical SEM and TEM display the nanooctahedra were grown on the ce-MoS2 sheets and average edge length of nanooctahedra was 100 ± 140 nm (Figure 2a-b). The HRTEM image of a nanooctahedron in the Cu_2O_{octa}-MoS_2 HNCs exhibits lattice fringes with a spacing of 0.24 nm, which matches well with that of the {111} planes of fcc Cu_2O. This indicates that {111}-facet-bounded Cu_2O nanooctahedra are contained in the Cu_2O_{octa}-MoS_2 HNCs (inset of Figure 2b).[24]

To investigate compositional structure of the HNCs, we performed the high-angle annular dark field scanning TEM (HAADF-STEM) and corresponding energy dispersive X-ray spectroscopy (EDS) measurement on Cu_2O_{cube}-MoS_2 and Cu_2O_{octa}-MoS_2 HNCs (Figure 3a-b). In part of Cu_2O NCs of the HNCs, compositional signals corresponding to Cu and oxygen are concentrated, while the signals of Mo and S are observed at 2D thin nanosheets, clearly demonstrating that growth of Cu_2O nanocubes and nanooctahedra on the ce-MoS_2 nanosheets for the Cu_2O_{cube}-MoS_2 and Cu_2O_{octa}-MoS_2 HNCs, respectively.

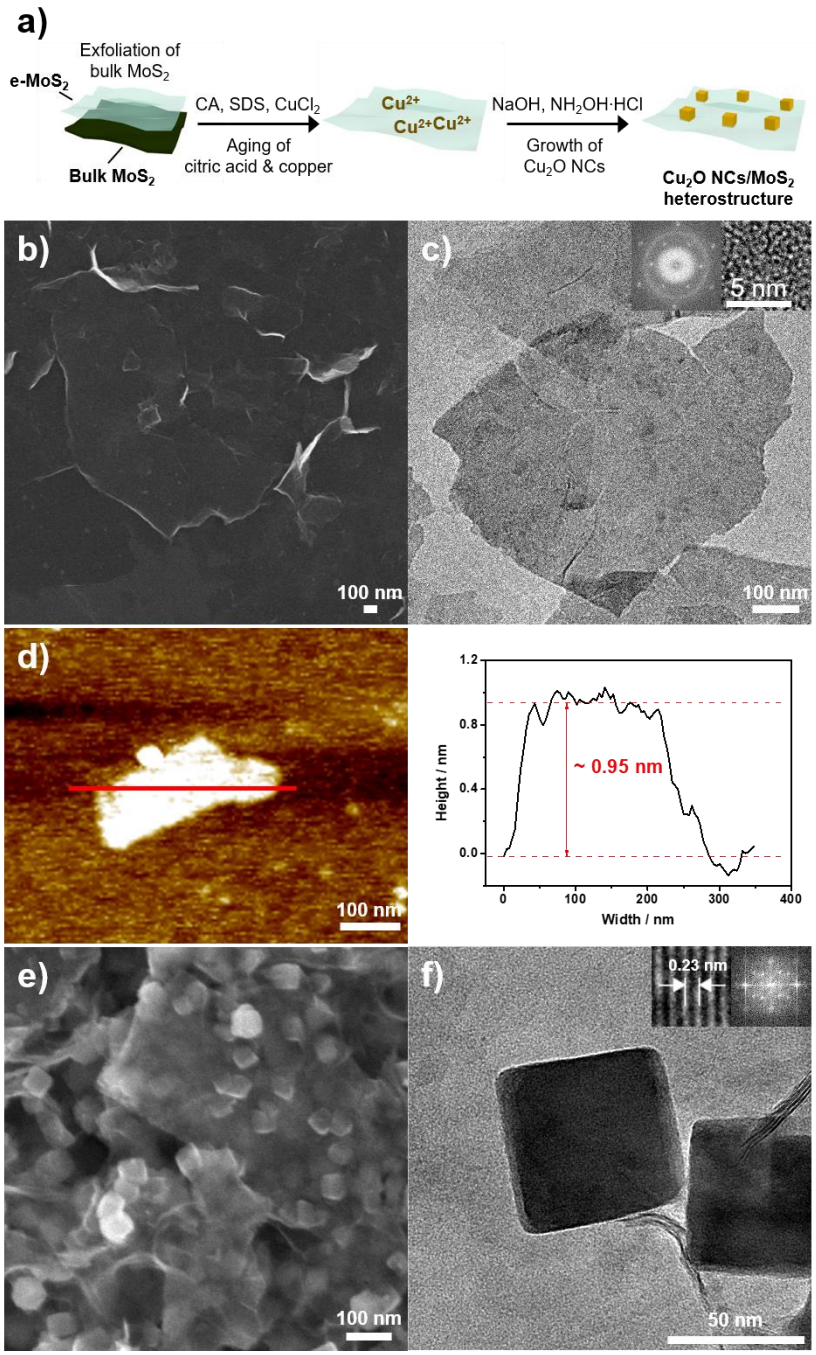

Figure 1. (a) Schematic illustration of the fabrication of Cu_2O_{cube}-MoS_2 HNCs. (b, c) SEM and TEM images of ce-MoS_2. (d) AFM images and corresponding height profiles of ce-MoS_2. (e, f) SEM and TEM images of Cu_2O_{cube}-MoS_2 HNCs.

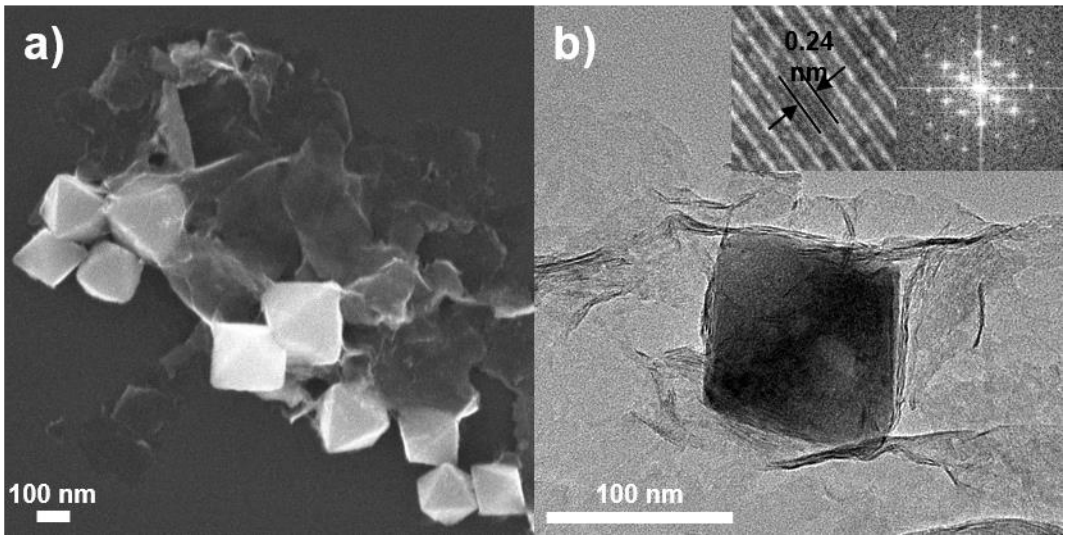

Figure 2. (a, b) SEM and TEM images of Cu_2O_{octa}-MoS_2 HNCs.

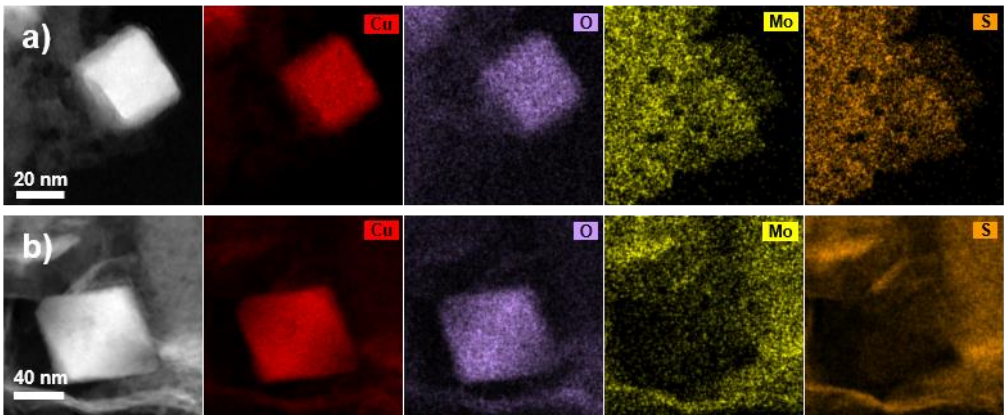

Figure 3. HAADF-STEM images and corresponding EDS elemental mapping images of (a) Cu_2O_{cube}-MoS_2 and (b) Cu_2O_{octa}-MoS_2 HNCs.

The X-ray diffraction (XRD) measurement was implemented to check the crystalline features of Cu_2O_{cube}-MoS_2 and Cu_2O_{octa}-MoS_2 HNCs. For both XRD patterns for the Cu_2O_{cube}-MoS_2 and Cu_2O_{octa}-MoS_2 HNCs, there are inherent peaks corresponding to cuprite structure of Cu_2O, which further corroborate the successful formation of Cu_2O_{cube}-MoS_2 and Cu_2O_{octa}-MoS_2 HNCs (Figure 4a). However, inherent peaks corresponding to hexagonal MoS_2 was not observed in the XRD pattern of ce-MoS_2 nanosheets, which might be attributed to low crystalline nature formed during chemically exfoliation procedure. In fact, the XRD patterns of the ce-MoS2 sheets by using larger amount of samples showed clear characteristic peaks corresponding to hexagonal crystalline structure (Figure 4b).

In addition, X-ray photoelectron spectroscopy (XPS) measurements on the Cu 2p core level of the Cu_2O_{octa}-MoS_2 HNCs verified that the Cu in the HNCs was almost in the Cu (I) state, whereas Cu_2O_{cube}-MoS_2 HNCs showed slightly larger amount of Cu (II) state.

The successful formation of Cu_2O_{cube}-MoS_2 HNCs with highly desirable structure for photocatalysis might be attributed to achievement of optimal growth kinetics of Cu_2O NCs on the ce-MoS_2 nanosheets by precisely manipulating the concentration ratios of [NaOH]/[NH_2OH•HCl]. In this system, NH_2OH•HCl can rapidly provide the electrons to $Cu(OH)_2$ for the formation of Cu_2O under appropriate concentration of OH- ions, while too high concentration of OH- ions promotes the formation of $Cu(OH)_2$ from $CuCl_2$ used as Cu precursor.[22,23]

In this synthetic system, Cu_2O NCs are produced through reduction of $Cu(OH)_2$ by NH_2OH•HCl, indicating that steady state concentration of $Cu(OH)_2$ is highly important for the growth and shape control of Cu_2O NCs. Since NaOH and NH_2OH•HCl can provide hydroxide ions (OH^-) and hydrogen ions (H^+), respectively, growth kinetics of Cu_2O NCs might be determined by concentration of [NaOH]/[NH_2OH•HCl] ratios. To corroborate the significance of concentration ratios of [NaOH]/[NH_2OH•HCl], series of experiments by employing various [NaOH]/[NH_2OH•HCl] ratios from 0.18 to 1.08 were carried out (where [NaOH]/[NH_2OH•HCl] ratios are changed by injecting different amount of NaOH, while amount of NH_2OH•HCl and other synthetic conditions for standard Cu_2O_{cube}-MoS_2 HNCs are unchanged). In the presence of [NaOH]/[NH_2OH•HCl] ratio of 0.18 in reaction mixture, no formation of new nanostructures was observed (Figure 6a). Similarly, increased [NaOH]/[NH_2OH•HCl] ratio of 0.24 produced the ill-defined NCs in the state before it became Cu_2O_{cube}-MoS_2 HNCs (Figure 6b). An increase in the [NaOH]/[NH_2OH•HCl] ratio of 0.36, which is the same [NaOH]/[NH_2OH•HCl] ratio used in the standard protocol, allowed to achievement of the Cu_2O_{cube}-MoS_2 HNCs (Figure 6c). In the present investigation, larger amount of NaOH was used to have a [NaOH]/[NH_2OH•HCl] ratio of 0.54, simultaneously leading to the growth of needle-like NCs and nanocubes on the ce-MoS_2 nanosheets (Figure 6d). When further increased to 0.72 and 1.08 of [NaOH]/[NH_2OH•HCl] ratios, only needle-like NCs instead of nanocubes were grown (Figure 6e,f), of which crystal structure is identified as CuO by XRD measurement (Figure 7a). Moreover, X-ray photoelectron spectroscopy (XPS) measurement on Cu 2p core level of the needle-like NCs identified that the Cu in the NCs was almost in the Cu^{2+} state (Figure 7b). In addition, [NaOH]/[NH_2OH•HCl] ratio-dependent growth trend of Cu oxide nanostructures was investigated by changing the amount of NH_2OH•HCl instead of NaOH, which also revealed similar growth behaviors of Cu oxide NCs (Figure 8). On the other hand, interestingly, absolute amount of NaOH and NH_2OH•HCl with

standard [NaOH]/[NH_2OH•HCl] ratios is also important for the formation of Cu_2O nanocubes. The higher concentration than that of standard condition allowed the formation of Cu_2O nanocubes (Figure 9a-c). In contrast, no formation of Cu_2O nanocubes was observed in lower concentration than that of standard condition (Figure 9d-f). These observations collectively demonstrate that controlling the growth kinetics of Cu oxide NCs by adjusting the amount of NaOH (or NH_2OH•HCl) versus NH_2OH•HCl (or NaOH) is the key point for regulating the shape and crystal structures of the Cu oxide-MoS_2 HNCs.

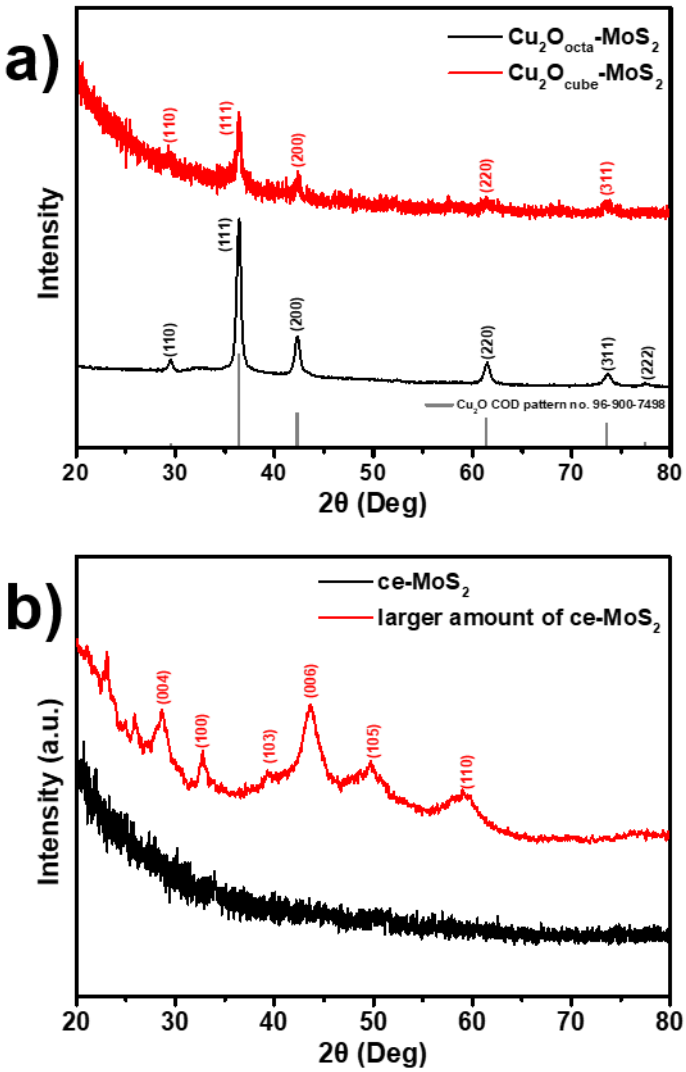

Figure 4. XRD pattern of (a) Cu_2O_{cube}-MoS_2 and Cu_2O_{octa}-MoS_2 HNCs, (b) ce-MoS_2 and larger amount of ce-MoS_2.

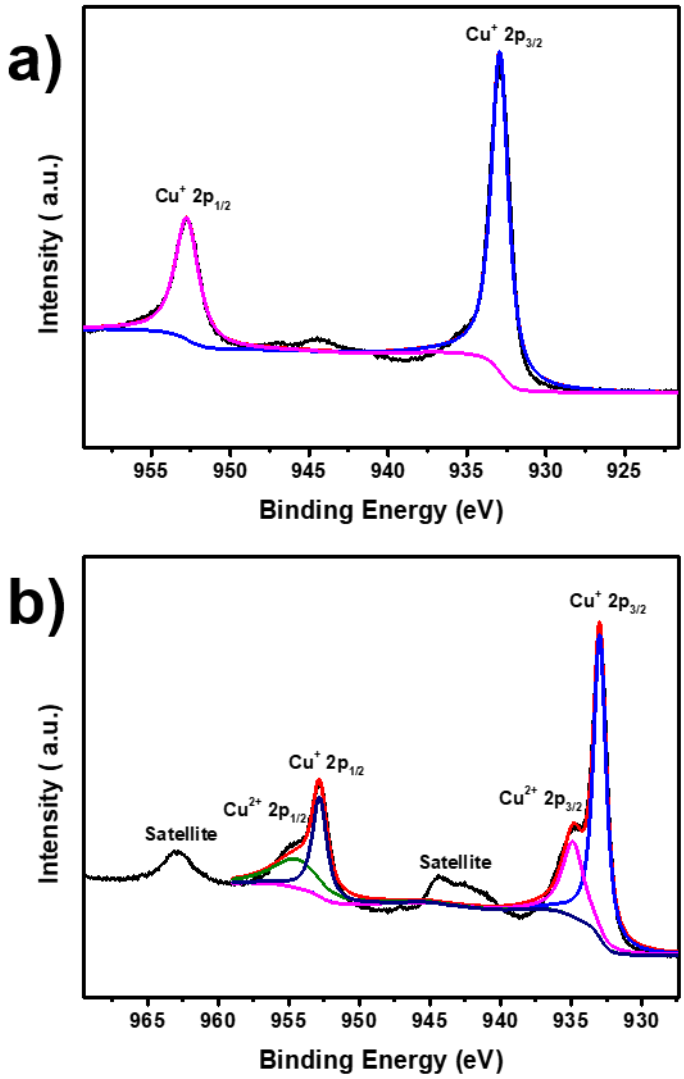

Figure 5. XPS spectra of (a) Cu_2O_{octa}-MoS_2 and (b) Cu_2O_{cube}-MoS_2 HNCs.

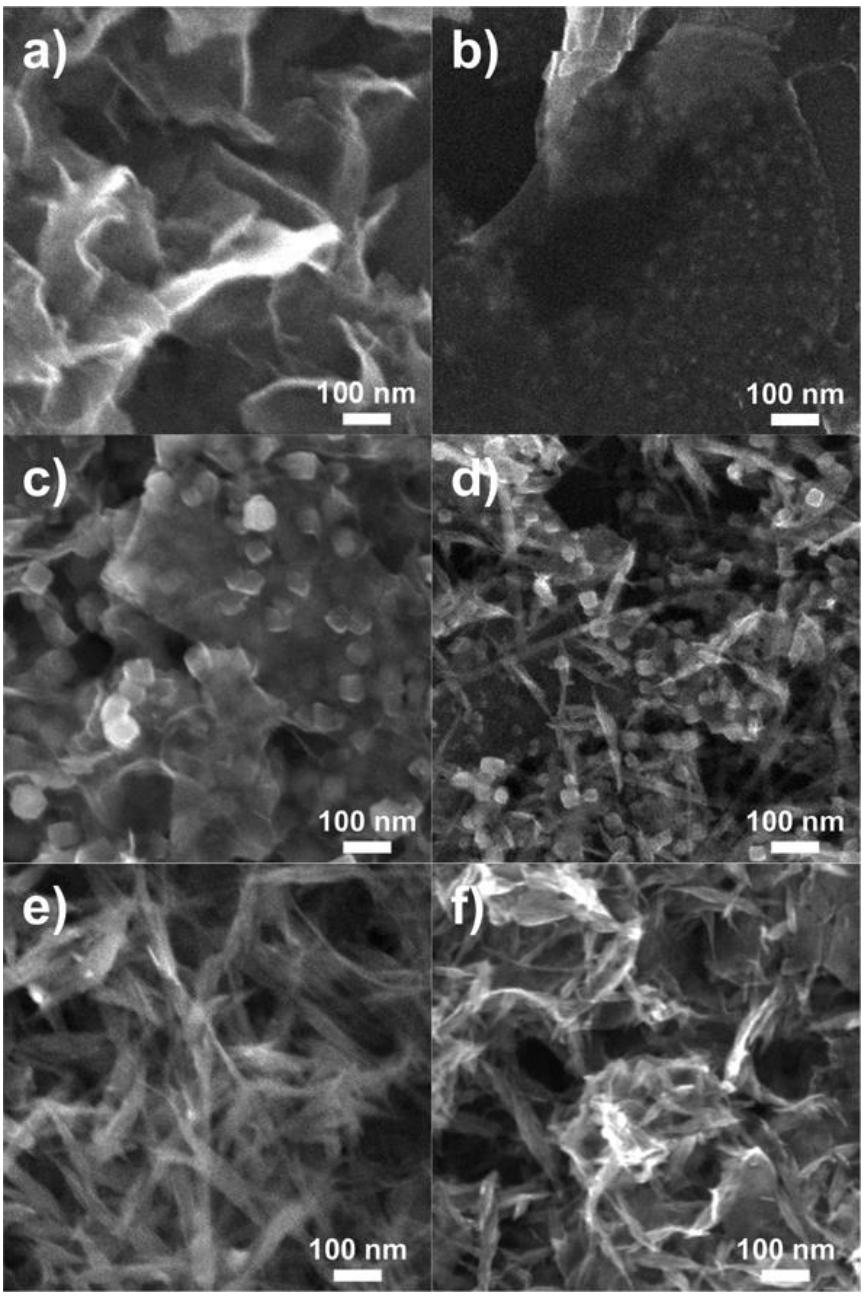

Figure 6. SEM images of Cu_2O_{cube}/MoS_2 according to the amount of NaOH (a) 36 μL, (b) 48 μL, (c) 72 μL, (d) 108 μL, (e) 144 μL and (f) 216 μL.

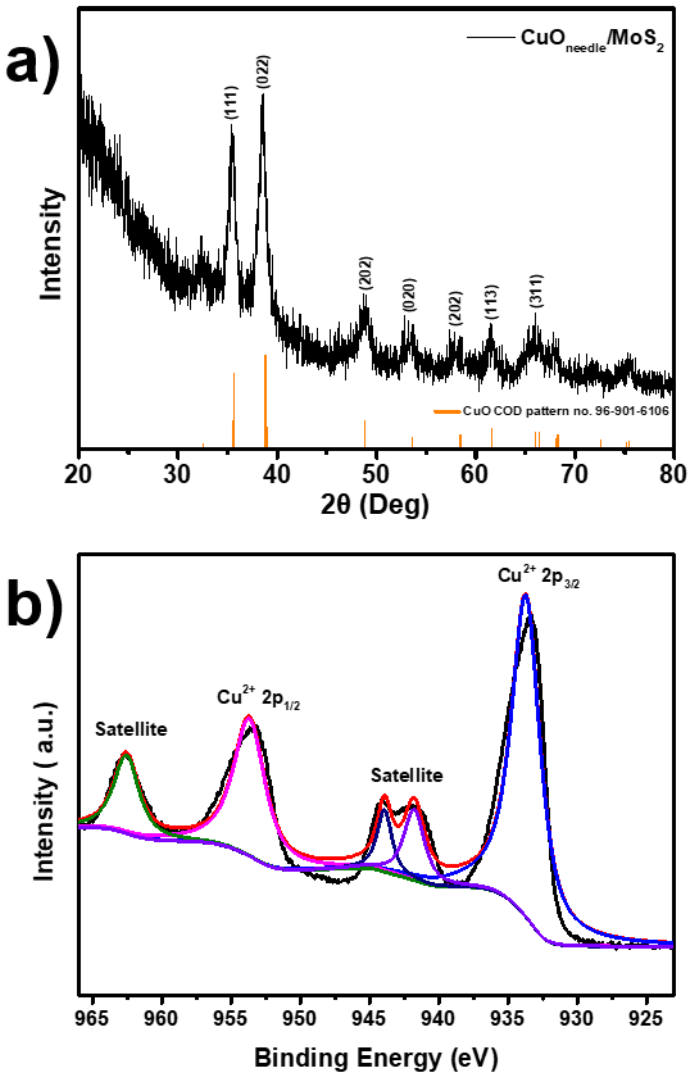

Figure 7. XRD pattern of (a) CuO_{needle}-MoS_2 and XPS spectra of (b) CuO_{needle}-MoS_2 HNCs.

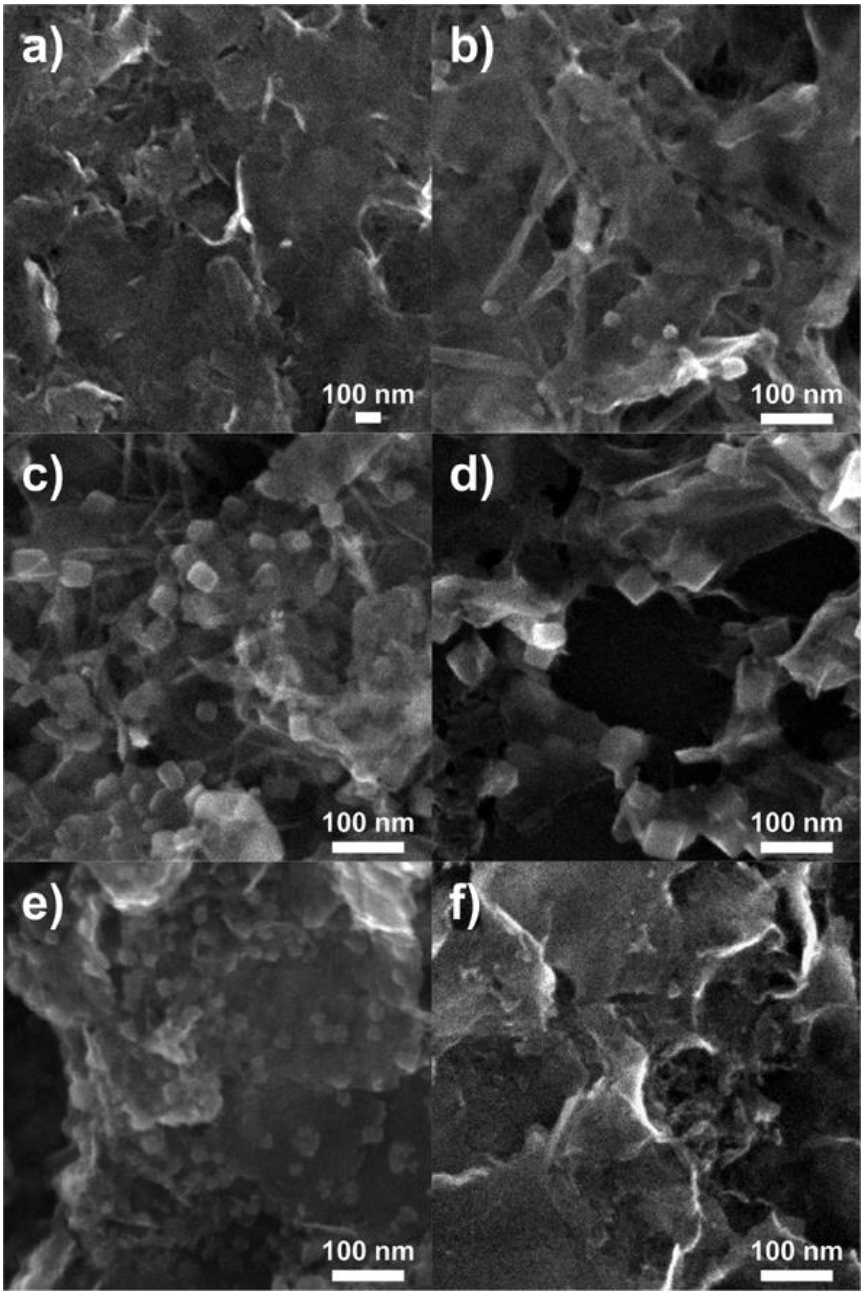

Figure 8. SEM images of Cu_2O_{cube}/MoS_2 according to the amount of $NH_2OH{\cdot}HCl$ (a) 80 μL, (b) 100 μL, (c) 133 μL, (d) 200 μL, (e) 400 μL and (f) 600 μL.

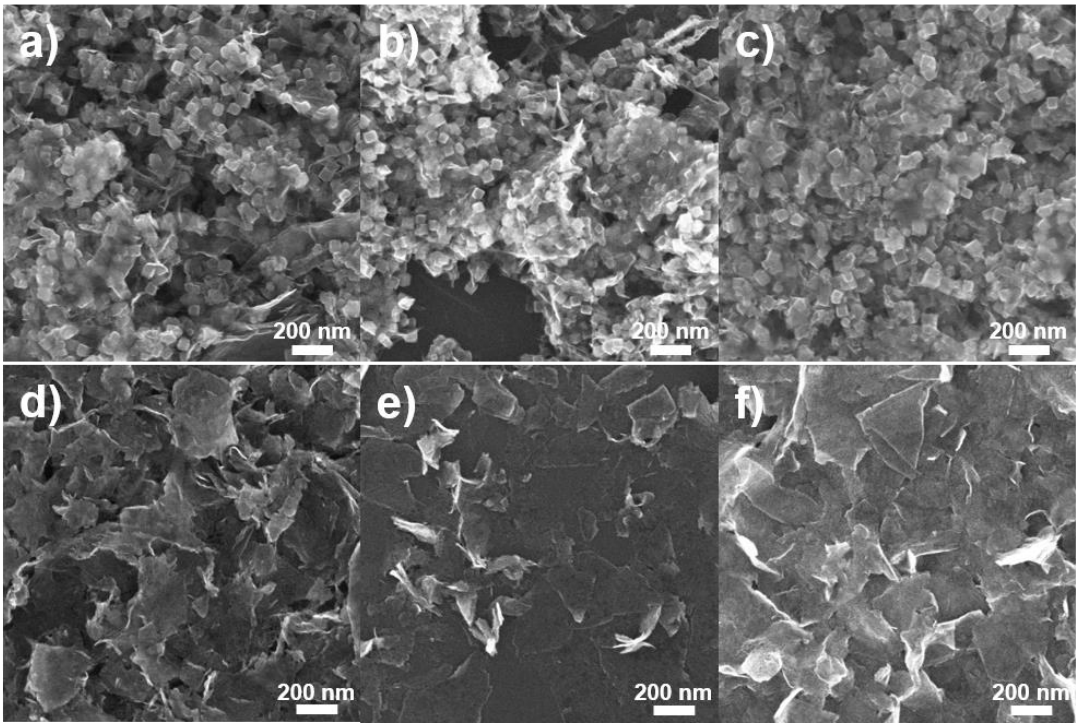

Figure 9. SEM images of Cu_2O_{cube}/MoS_2 according to the ratio of NaOH and $NH_2OH{\cdot}HCl$ (a) 1.2, (b) 1.6, (c) 2.2, (d) 0.8, (e) 0.5 and (f) 0.2 times.

To further elucidate the efficient separation and retarded recombination of phot-induced charge carriers in the Cu_2O_{cube}-MoS_2 HNCs, photoluminescence (PL) measurement was implemented over Cu_2O_{cube}-MoS_2 HNCs, Cu_2O_{octa}-MoS_2 HNCs, Cu_2O_{sphere}-MoS_2, CuO_{needle}-MoS_2 HNCs, Cu_2O nanocubes, and Cu_2O nanooctahedra. Cu_2O_{cube}-MoS_2 HNCs, Cu_2O_{octa}-MoS_2 HNCs showed much lower PL emission intensity compared with pure Cu_2O nanocubes and nanooctahedra (Figure 10), indicating that formation of intimate heterojection of Cu_2O NCs and ce-MoS_2 nanosheets can advance the migration and extension the life-time of the charge carriers and frustrate the combination of photo-induced charge carriers. Meanwhile, the most effective separation of photo-induced carriers and charge recombination may lead to the lowest PL intensity of the Cu_2O_{cube}-MoS_2 HNCs, which in further improving the photocatalytic activity.

Figure 11 shows UV-vis absorption spectra of the Cu_2O_{cube}-MoS_2 HNCs, Cu_2O nanocubes, and ce-MoS_2 nanosheets. The UV-vis spectrum of Cu_2O nanocubes exhibits a maximum absorption peak at around 600 nm[25] owing to its band gap of 2.2 eV, which is estimated by Kubelka-Munk method.[26] The UV-vis spectrum of ce-MoS_2 nanosheets presents a big peak at 250-300 nm. In contrast to Cu_2O nanocubes, Cu_2O_{cube}-MoS_2 HNCs showed enhanced intensity of absorption in the range of 200 to 800 nm, which may be assigned to ce-MoS_2 nanosheets in the Cu_2O_{cube}-MoS_2 HNCs. These results showed that efficient light absorption of the Cu_2O_{cube}-MoS_2 HNCs can be achieved due to combination of Cu_2O nanocubes and ce-MoS_2 nanosheets, which can lead to improved light harvesting efficiency.

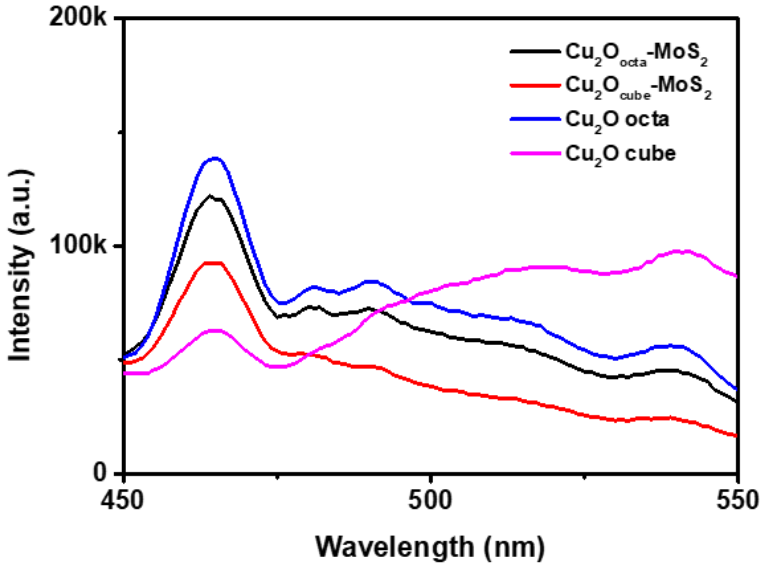

Figure 10. PL spectra of Cu_2O_{octa}-MoS_2, Cu_2O_{cube}-MoS_2, Cu_2O nanooctahedra and Cu_2O nanocubes.

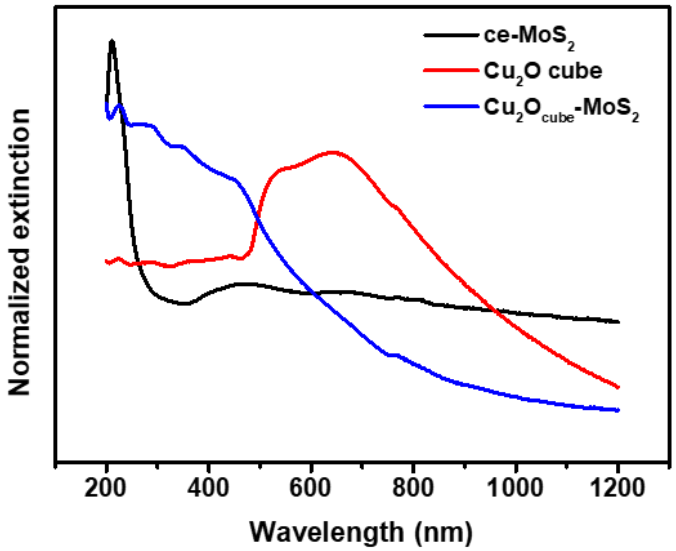

Figure 11. UV-vis spectra of ce-MoS_2, Cu_2O NCs and Cu_2O_{cube}-MoS_2 HNCs.

III-2. Photocatalytic Property and Mechanisms

For investigating the photocatalytic performances of Cu_2O_{cube}-MoS_2 and Cu_2O_{octa}-MoS_2 HNCs depending on their exposed Cu_2O surface and anisotropic morphology, degradation of theophylline, which is one of important pharmaceutical molecule, were conducted with Cu_2O_{cube}-MoS_2 HNCs, Cu_2O_{octa}-MoS_2 HNCs, Cu_2O_{sphere}-MoS_2 HNCs, CuO_{needle}-MoS_2 HNCs, Cu_2O nanocubes, Cu_2O nanooctahedra, ce-MoS_2 nanosheets, and physical mixture of Cu_2O nanocubes/ce-MoS_2 nanosheets under dark and visible light irradiation ($\lambda > 400$ nm) and their photocatalytic activities were compared with those of various types of catalysts.

The Cu_2O_{sphere}-MoS_2 and CuO_{needle}-MoS_2 HNCs were prepared by directly growing of Cu_2O nanospheres or CuO nanoneedles instead of Cu_2O nanocubes on ce-MoS_2 nanosheets, respectively (Figure 12a-b). In the dark, all photocatalysts revealed negligible (slight) decrease of concentration changes of theophylline (Figure 13a), while significant degradation of theophylline was observed under light irradiation, clearly indicating that significant decrease of intensity of C/C_0 may be mainly attributed to photocatalytic process. Figure 13b-c shows the normalized concentration changes in theophylline (C/C_0) versus irradiation time for the different photocatalysts and corresponding kinetic constant of photocatalytic degradation of theophylline, respectively. From theophylline degradation experiments implemented under light irradiation, photocatalytic activities of the photocatalysts follow the order Cu_2O_{cube}-MoS_2 HNCs > Cu_2O_{octa}-MoS_2 HNCs > Cu_2O_{sphere}-MoS_2 HNCs > Cu_2O nanooctahedra > CuO_{needle}-MoS_2 HNCs > Cu_2O nanocubes > physical mixture of Cu_2O nanocubes and ce-MoS_2 nanosheets > ce-MoS_2 nanosheets. It is worth noting that all Cu_2O-MoS_2 HNCs significantly improved the rate of theophylline degradation compared to their single semiconductor counterparts, and physical mixture of Cu_2O nanocubes and ce-MoS_2 nanosheets. The better photocatalytic performances for Cu_2O-MoS_2 HNCs are attributed to formation of intimate coupling of Cu_2O and MoS_2, which improve light absorption efficiency, migration of charge carriers, and prevent the recombination of photo-induced charge carriers. Physical mixture of Cu_2O nanocubes and ce-MoS_2 nanosheets presented slightly deteriorated activity as compared with Cu_2O nanocubes, clearly demonstrating the importance of intimate heterojunction between Cu_2O and MoS_2. Meanwhile, lower photocatalytic activity of CuO_{needle}-MoS_2 HNCs than Cu_2O_{cube}-MoS_2 and Cu_2O_{sphere}-MoS_2 HNCs implies that types of crystal structure of Cu oxide NCs could also influence on its photocatalytic activity. As such, the higher

photocatalytic activities of the Cu_2O-MoS_2 HNCs than that of the CuO_{needle}-MoS_2 HNCs can be attributed to desirable band structure of Cu_2O (band gaps of Cu_2O and CuO are 2.2 and 1.58 eV, respectively)[27] for effectively absorbing visible light and adequate CB/VB potential edges of Cu_2O NCs in the Cu_2O_{cube}-MoS_2 HNCs compared with those of CuO in CuO_{needle}-MoS_2 HNCs for theophylline degradation.

Beside the intimate heterojuction of Cu_2O NCs and ce-MoS_2 nanosheets, we found that the photocatalytic performances of the Cu_2O-MoS_2 HNCs are highly dependent on exposed plane of Cu_2O NCs in the HNCs. Indeed, Cu_2O_{cube}-MoS_2 HNCs with {100} facet-terminated Cu_2O nanocubes greatly improved rate of theophylline degradation than Cu_2O_{sphere}-MoS_2 HNCs with random-facets of Cu_2O NCs, which is higher than that of Cu_2O_{sphere}-MoS_2 HNCs based on Pseudo-first-order kinetic plots (Figure 13c), although Cu_2O_{sphere}-MoS_2 HNCs were constructed by using identical ce-MoS_2 nanosheets as 2D template like the Cu_2O_{cube}-MoS_2 HNCs.

To further check the above influence of compositional and surface-morphological properties over photocatalytic pollutant degradation, we estimated photocatalytic degradation of methyl orange under visible light by using 400 nm cut on filter. Similar trends of photocatalytic performances of the photocatalyts were further observed for degradation of methyl orange (Figure 13d-f), demonstrating the significance of intimate contact of Cu_2O_{cube}-MoS_2 HNCs by direct-growth of Cu_2O NCs on ce-MoS_2 nanosheets for enhancement over its photocatalytic performance, which can facilitate the achievement of the synergistic benefits such wide range of light absorption and efficient migration of charge carriers.

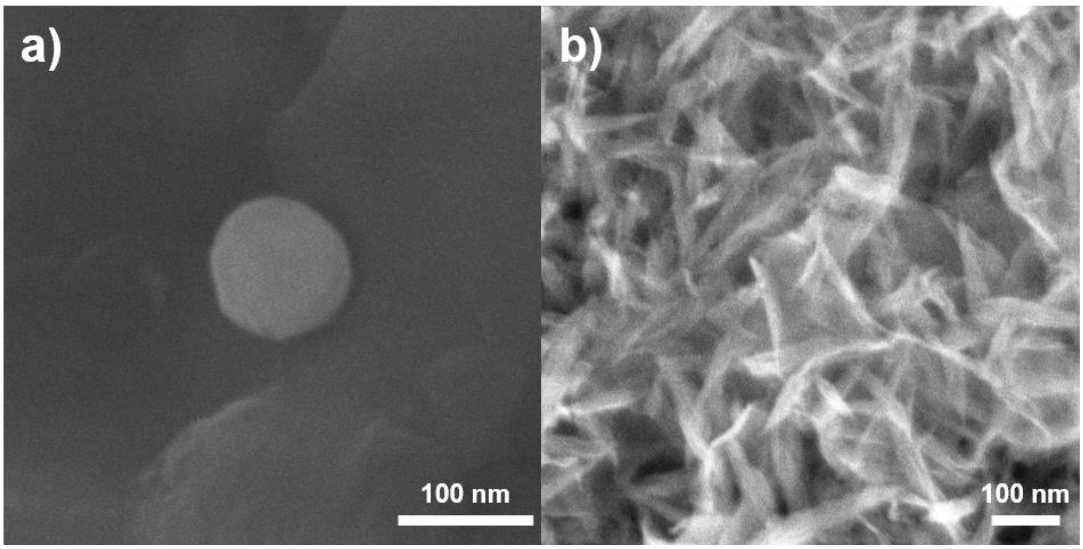

Figure 12. SEM images of (a) Cu_2O_{sphere}-MoS_2 and (b) CuO_{needle}-MoS_2 HNCs.

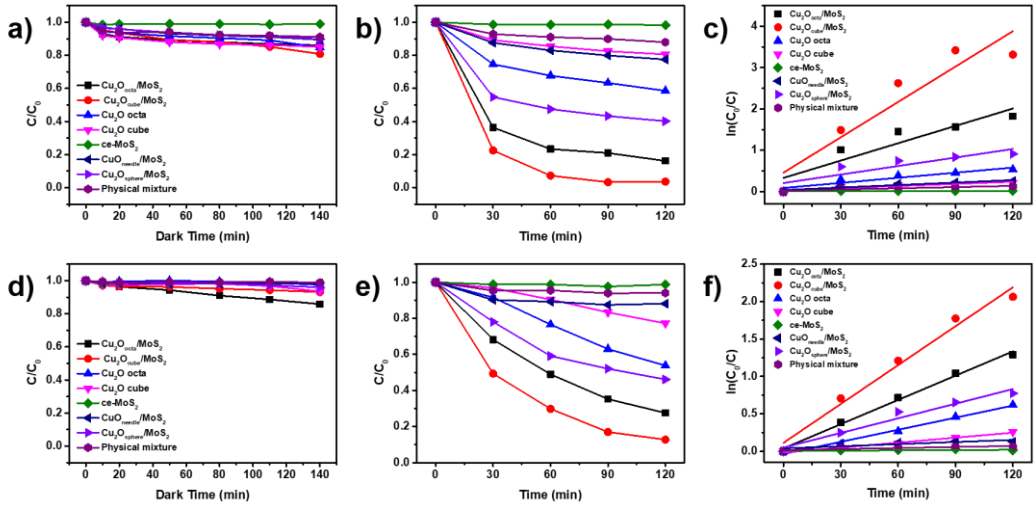

Figure 13. Photocatalytic degradation of theophylline (a) in dark, (b, c) under visible light irradiation and methyl orange (d) in dark, (e, f) under visible light irradiation.

To investigate the photocatalytic mechanism of the Cu_2O-MoS_2 photocatalyst in the degradation process, several main reactive radical species is examined by radical trapping experiment, as shown in Fig. 14. Considering that radicals produced via electron- and hole-induced processes promote removal of pollutants, introduction of electron/hole scavengers can selectively suppress the formation of each radicals by electron- and hole-induced processes, which can allow the dominant photocatalytic process and active radicals for degradation of pollutants. For investigation, degradation rate of theophylline was estimated in the presence of $K_2Cr_2O_7$ and KI used as electron and hole scavengers, respectively.[28] As shown in Fig 14a and 14b, photocatalytic activity of the Cu_2O_{cube}-MoS_2 HNCs and Cu_2O nanocubes with addition of $K_2Cr_2O_7$ was remarkably lower than that measured in absent of electron scavengers. In contrast, introduction of hole scavenger (KI) barely influenced to photocatalytic activity of the Cu_2O_{cube}-MoS_2 HNCs and Cu_2O nanocubes. In addition, similar trend was also obtained in control experiments for methyl orange degradation (Figure 14c), clearly indicating that $\bullet O_2^-$ radicals formed by electron-induced process play a crucial role for theophylline and methyl orange degradation.

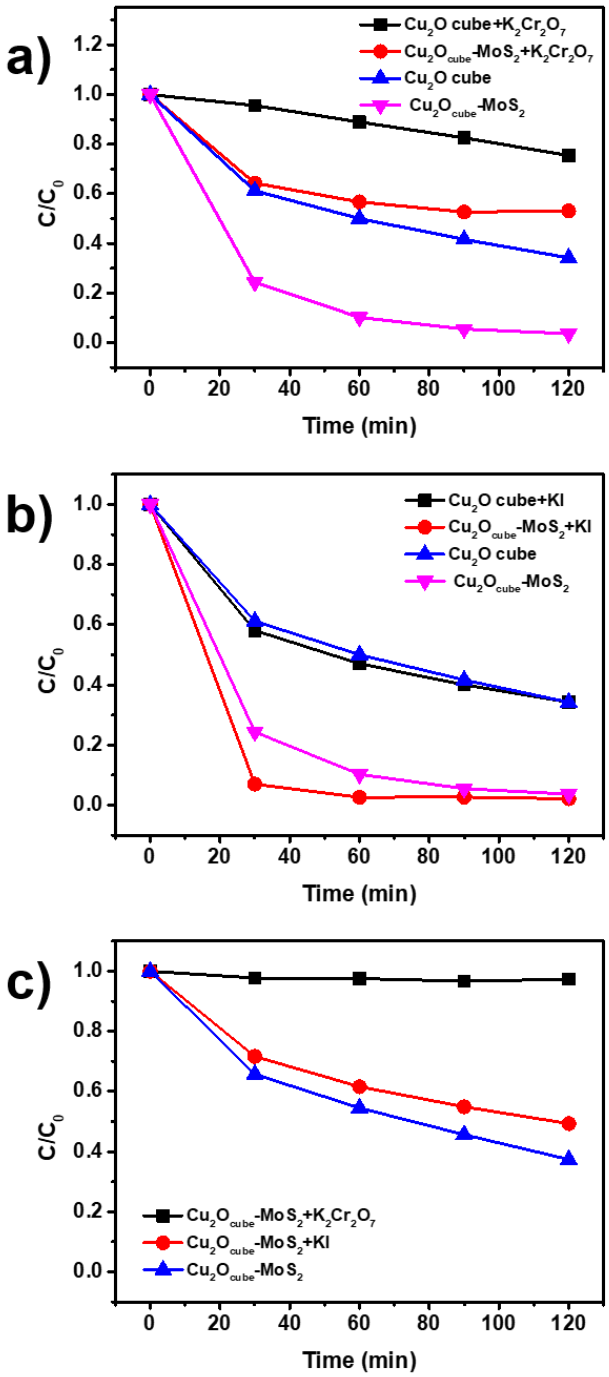

Figure 14. Photocatalytic degradation of (a, b) theophylline and (c) methyl orange with different trapping agent under visible light.

In order to further prove the active species produced in the photocatalytic system, spin-trapping ESR analyses[28,29] over pure Cu_2O and Cu_2O-MoS_2 is used with 5,5-dimethyl-1-pyrriline N-Oxide (DMPO). Typically, DMPO can form a radical scavenger of stable DMPO − •O_2^- or DMPO − •OH species with •O_2^- or •OH generated in the system, respectively and the results are presented in Fig. 15a-b. With the visible light illumination, the Cu_2O cube, Cu_2O octa, Cu_2O_{cube}-MoS_2 and Cu_2O_{octa}-MoS_2 exhibit peaks of the DMPO − •O_2^- adduct in Fig. 15a. The peaks of Cu_2O_{cube}-MoS_2 obviously show stronger intensities, indicating that the •O_2^- has been generated via the reduction of O_2 and Cu_2O combined with CuO could contribute to produce more •O_2^- radical species.[30-32] Meanwhile, the signals of the DMPO − •OH over Cu_2O_{cube}-MoS_2 have no obvious ESR signals compare with other catalysts (Figure 15b). It means that partial of h+ prefers to participate in the direct oxidation reaction for the Cu_2O-MoS_2 system. Therefore, together with the previous radical trapping experiment, the main active species is proved to be the superoxide radical in the photocatalytic degradation process of theophylline and methyl orange.

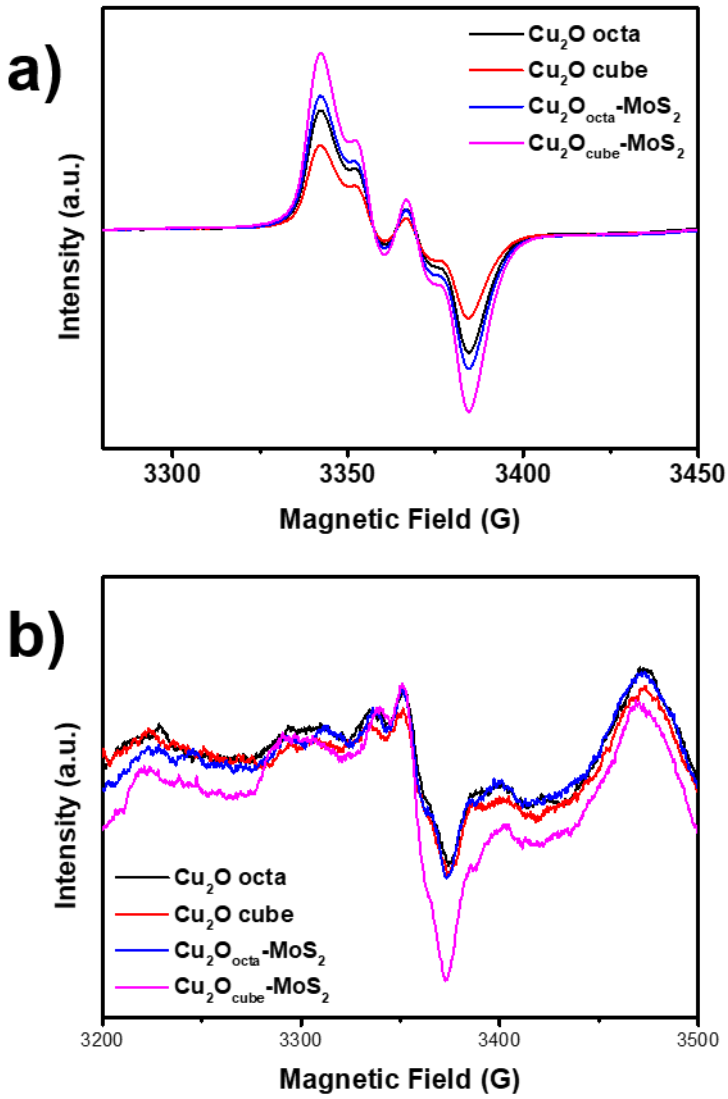

Figure 15. DMPO spin-trapping ESR spectra of Cu_2O nanooctahedra, Cu_2O nanocubes, Cu_2O_{octa}-MoS_2 and Cu_2O_{cube}-MoS_2 HNCs (a) methanol dispersion for DMPO − •O_2^- (b) and aqueous dispersion for DMPO − •OH.

Furthermore, to understand mechanism of pollutant degradation[33,34] in the Cu_2O_{cube}-MoS_2 HNCs, band structure of Cu_2O_{cube}-MoS_2 HNCs was first constructed using Kubelka-Munk method based on diffuse reflectance spectroscopy of pristine Cu_2O and ce-MoS_2 nanosheets (Figure 16). The band gaps of Cu_2O and ce-MoS_2 nanosheets are 2.2 and 1.75 eV, respectively, which allowed the establishment of band diagram of the Cu_2O_{cube}-MoS_2 HNCs (Figure 16c). According to band structures of the Cu_2O_{cube}-MoS_2 HNCs, photo-induced electrons in the CB of Cu_2O nanocubes spontaneously flow to CB of ce-MoS_2 nanosheets due to more negative potential of CB edge of Cu_2O nanocubes than that of ce-MoS_2 nanosheets under irradiation (Process 1 in Figure 17). Meanwhile photo-induced holes are accumulated in the VB of Cu_2O nanocubes by formation of holes in VB of Cu_2O nanocubes by light absorption and migration of photo-induced holes from VB of ce-MoS_2 nanosheets (Process 2 in Figure 17). The $\bullet O_2^-$ and •OH radicals are formed by reaction with photo-induced electrons and O_2, while the holes tend to produce •OH radicals by reacting with H_2O. Overall, electron- and hole-induced processes can provide $\bullet O_2^-$ and •OH radicals that are major radical species to remove pollutants such as theophylline and MO. The possible migration of charge carriers formed in the Cu_2O_{cube}-MoS_2 HNCs and reactions with pollutant molecules charge carriers were postulated as shown in Figure 17 and following equations:

Electron-induced pollutant removal process:

Cu_2O_{cube}-MoS_2 HNCs + hv → e^- (Cu_2O nanocubes) + h^+ (ce-MoS_2 nanosheets)

e^- (Cu_2O nanocubes) $_{CB}$ → e^- (ce-MoS_2 nanosheets) $_{CB}$

e^- (ce-MoS_2 nanosheets) $_{CB}$ + O_2 → $\bullet O_2^-$

e^- (ce-MoS_2 nanosheets) $_{CB}$ + O_2 + $2H^+$ → H_2O_2

H_2O_2 → •OH + OH^-

Pollutants (MO and theophylline) + $\bullet O_2^-$ → degradation

Pollutants (MO and theophylline) + •OH → degradation

Hole-induced pollutant removal process:

h^+ (ce-MoS_2 nanosheets) $_{VB}$ → h^+ (Cu_2O nanocubes) $_{VB}$

h^+ (Cu_2O nanocubes) $_{VB}$ + H_2O → •OH + H^+

Pollutants (MO and theophylline) + •OH → degradation

On basis of the above mechanism and the experimental results, the enhanced photocatalytic performance of Cu_2O_{cube}-MoS_2 composites can be ascribed to the synergic effect of the efficient separation of the light generating electron-hole pairs due to intimate bonding of Cu_2O and MoS_2 and increased surface area.

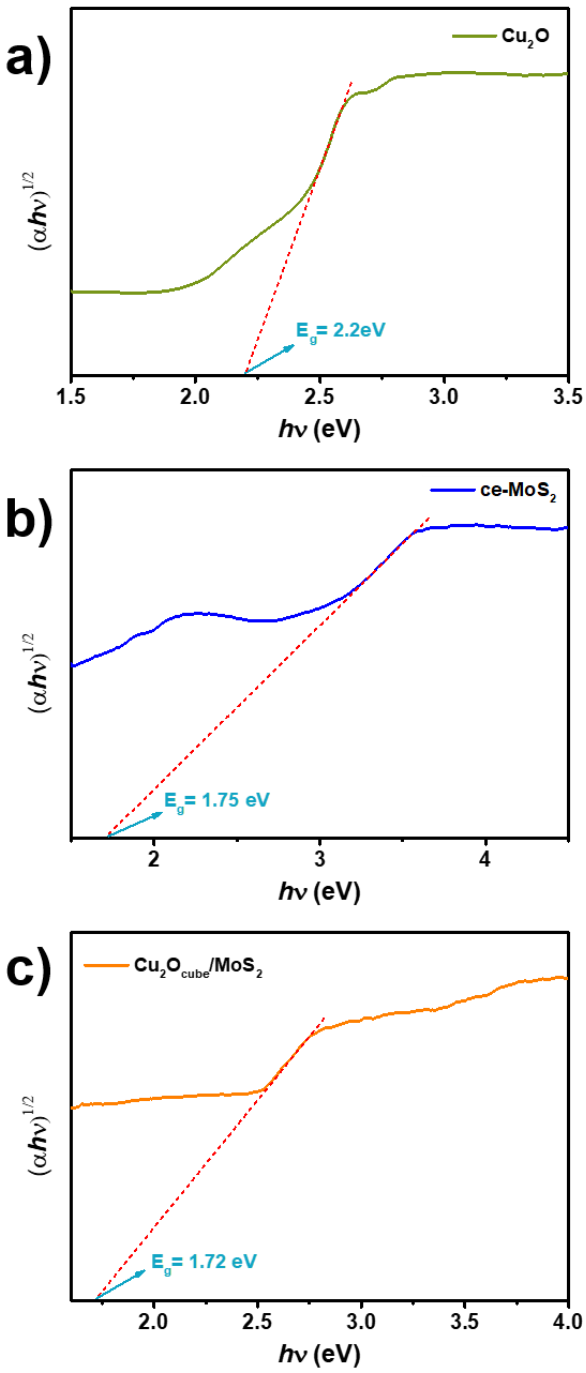

Figure 16. The estimated band gap energies of (a) Cu_2O, (b) ce-MoS_2 and (c) Cu_2O_{cube}-MoS_2 HNCs.

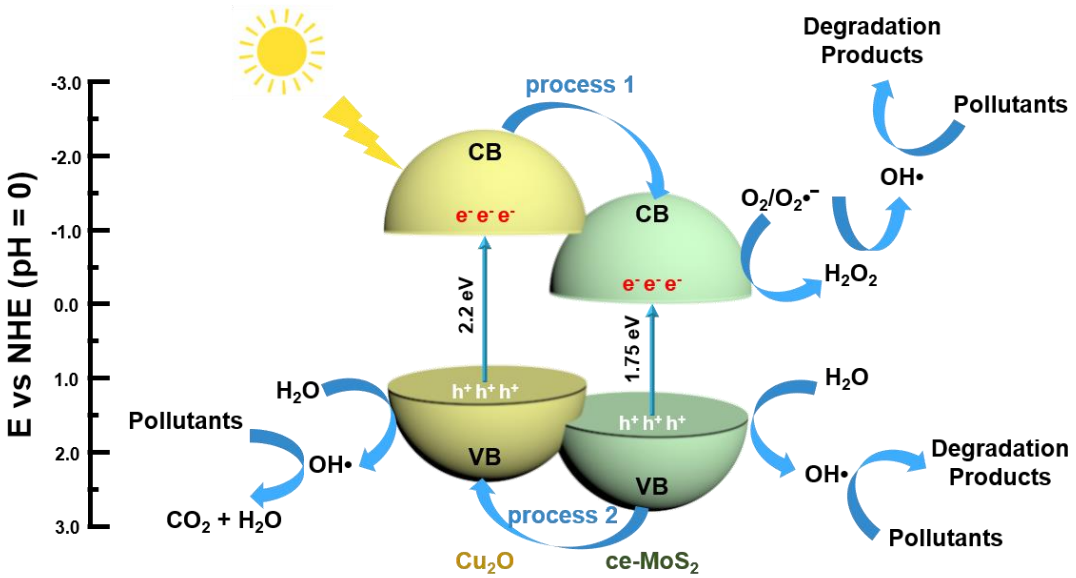

Figure 17. Proposed mechanism for the photocatalytic degradation of pollutants over Cu_2O-MoS_2 HCNs under visible light irradiation.

IV. Conclusion

In summary, Cu_2O-MoS_2 was synthesized by growing several photocatalysts on MoS_2 nanosheets using a simple synthesis method. Cu_2O-MoS_2 nanocomposites were used to investigate the photocatalytic decomposition of contaminants in water. Compared to pure nanoparticles and other shaped Cu_2O and CuO materials, Cu_2O_{cube}-MoS_2 has been shown to exhibit excellent photocatalytic activity against the degradation of theophylline and methyl orange under visible light ($\lambda \geq 400$ nm). This may be due to the increased light absorption intensity and the efficient separation of the light generating electron-hole pairs and the synergistic effect of the increased surface area due to the composite structure. Appropriate mechanisms for enhanced photocatalytic activity of Cu_2O_{cube}-MoS_2 have been proposed with detailed description.

This study is expected to provide a simple strategy for the manufacture and development of visible light photocatalysts for environmental protection as well as potential industrial applications for the decomposition of contaminated wastewater.

V. Reference

1. Clifford, John N., Emilio Palomares, Md K. Nazeeruddin, Ravindranathan Thampi, Michael Grätzel, and James R. Durrant. "Multistep electron transfer processes on dye co-sensitized nanocrystalline TiO_2 films." *Journal of the American Chemical Society* 126, no. 18 (2004): 5670-5671.
2. Chen, Chuncheng, Wanhong Ma, and Jincai Zhao. "Semiconductor-mediated photodegradation of pollutants under visible-light irradiation." *Chemical Society Reviews* 39, no. 11 (2010): 4206-4219.
3. Lin, Haifeng, Liping Li, Minglei Zhao, Xinsong Huang, Xiaomei Chen, Guangshe Li, and Richeng Yu. "Synthesis of high-quality brookite TiO_2 single-crystalline nanosheets with specific facets exposed: tuning catalysts from inert to highly reactive." *Journal of the American chemical society* 134, no. 20 (2012): 8328-8331.
4. Ort, Christoph, Michael G. Lawrence, Jorg Rieckermann, and Adriano Joss. "Sampling for pharmaceuticals and personal care products (PPCPs) and illicit drugs in wastewater systems: are your conclusions valid? A critical review." *Environmental science & technology* 44, no. 16 (2010): 6024-6035.
5. Martínez, C. M. C. L., M. I. Fernández, J. A. Santaballa, and J. Faria. "Kinetics and mechanism of aqueous degradation of carbamazepine by heterogeneous photocatalysis using nanocrystalline TiO_2, ZnO and multi-walled carbon nanotubes–anatase composites." *Applied Catalysis B: Environmental* 102, no. 3-4 (2011): 563-571.
6. Snyder, Shane A., Paul Westerhoff, Yeomin Yoon, and David L. Sedlak. "Pharmaceuticals, personal care products, and endocrine disruptors in water: implications for the water industry." *Environmental engineering science* 20, no. 5 (2003): 449-469.
7. Joss, Adriano, Henrik Andersen, Thomas Ternes, Philip R. Richle, and Hansruedi Siegrist. "Removal of estrogens in municipal wastewater treatment under aerobic and anaerobic conditions: consequences for plant optimization." *Environmental science & technology* 38, no. 11 (2004): 3047-3055.
8. Snyder, Shane A., Eric C. Wert, David J. Rexing, Ronald E. Zegers, and Douglas D. Drury. "Ozone oxidation of endocrine disruptors and pharmaceuticals in surface water and wastewater." *Ozone: Science and Engineering* 28, no. 6 (2006): 445-460.
9. Westerhoff, Paul, Yeomin Yoon, Shane Snyder, and Eric Wert. "Fate of endocrine-disruptor,

pharmaceutical, and personal care product chemicals during simulated drinking water treatment processes." *Environmental science & technology* 39, no. 17 (2005): 6649-6663.

10. Hu, A., X. Zhang, D. Luong, K. D. Oakes, M. R. Servos, R. Liang, S. Kurdi, P. Peng, and Y. Zhou. "Adsorption and photocatalytic degradation kinetics of pharmaceuticals by TiO_2 nanowires during water treatment." *Waste and Biomass Valorization* 3, no. 4 (2012): 443-449.
11. Bai, Jing, Yanbiao Liu, Jinhua Li, Baoxue Zhou, Qing Zheng, and Weimin Cai. "A novel thin-layer photoelectrocatalytic (PEC) reactor with double-faced titania nanotube arrays electrode for effective degradation of tetracycline." *Applied Catalysis B: Environmental* 98, no. 3-4 (2010): 154-160.
12. Calza, Paola, V. A. Sakkas, A. Villioti, Cristina Massolino, V. Boti, Ezio Pelizzetti, and T. Albanis. "Multivariate experimental design for the photocatalytic degradation of imipramine: Determination of the reaction pathway and identification of intermediate products." *Applied Catalysis B: Environmental* 84, no. 3-4 (2008): 379-388.
13. Wu, Li-Cheng, Hang Zhao, Li-Guo Jin, and Huan-Yan Xu. "TiO_2/gC_3N_4 heterojunctions: In situ fabrication mechanism and enhanced photocatalytic activity." *Frontiers of Materials Science* 10, no. 3 (2016): 310-319.
14. Wang, Yajun, Qisheng Wang, Xueying Zhan, Fengmei Wang, Muhammad Safdar, and Jun He. "Visible light driven type II heterostructures and their enhanced photocatalysis properties: a review." *Nanoscale* 5, no. 18 (2013): 8326-8339.
15. Zhang, Jinshui, Mingwen Zhang, Rui-Qing Sun, and Xinchen Wang. "A facile band alignment of polymeric carbon nitride semiconductors to construct isotype heterojunctions." *Angewandte Chemie International Edition* 51, no. 40 (2012): 10145-10149.
16. Chu, Chieh-Yu, and Michael H. Huang. "Facet-dependent photocatalytic properties of Cu_2O crystals probed by using electron, hole and radical scavengers." *Journal of Materials Chemistry A* 5, no. 29 (2017): 15116-15123.
17. Kim, Chang Woo, So Jin Yeob, Hui-Ming Cheng, and Young Soo Kang. "A selectively exposed crystal facet-engineered TiO_2 thin film photoanode for the higher performance of the photoelectrochemical water splitting reaction." *Energy & Environmental Science* 8, no. 12 (2015): 3646-3653.
18. Harn, Yeu-Wei, Tung-Han Yang, Tsung-Yeh Tang, Miao-Chun Chen, and Jenn-Ming Wu. "Facet-Dependent Photocatalytic Activity and Facet-Selective Etching of Silver (I) Oxide Crystals with Controlled Morphology." *ChemCatChem* 7, no. 1 (2015): 80-86.

19. Hong, Jong Wook, Dae Han Wi, Su-Un Lee, and Sang Woo Han. "Metal–semiconductor heteronanocrystals with desired configurations for plasmonic photocatalysis." *Journal of the American Chemical Society* 138, no. 48 (2016): 15766-15773.
20. Xu, You, Huan Wang, Yifu Yu, Lei Tian, Weiwei Zhao, and Bin Zhang. "Cu_2O nanocrystals: surfactant-free room-temperature morphology-modulated synthesis and shape-dependent heterogeneous organic catalytic activities." *The Journal of Physical Chemistry C* 115, no. 31 (2011): 15288-15296.
21. Wi, Dae Han, Se Young Park, Seunghoon Lee, Jiha Sung, Jong Wook Hong, and Sang Woo Han. "Metal–semiconductor ternary hybrids for efficient visible-light photocatalytic hydrogen evolution." *Journal of Materials Chemistry A* 6, no. 27 (2018): 13225-13235.
22. Gou, Linfeng, and Catherine J. Murphy. "Solution-phase synthesis of Cu_2O nanocubes." *Nano Letters* 3, no. 2 (2003): 231-234.
23. Kumar, Santosh, Christopher MA Parlett, Mark A. Isaacs, Danielle V. Jowett, Richard E. Douthwaite, Martin CR Cockett, and Adam F. Lee. "Facile synthesis of hierarchical Cu_2O nanocubes as visible light photocatalysts." *Applied Catalysis B: Environmental* 189 (2016): 226-232.
24. He, Ping, Xinghai Shen, and Hongcheng Gao. "Size-controlled preparation of Cu_2O octahedron nanocrystals and studies on their optical absorption." *Journal of Colloid and Interface Science* 284, no. 2 (2005): 510-515.
25. Li, Benxia, Tongxuan Liu, Luyang Hu, and Yanfen Wang. "A facile one-pot synthesis of Cu_2O/RGO nanocomposite for removal of organic pollutant." *Journal of Physics and Chemistry of Solids* 74, no. 4 (2013): 635-640.
26. Christy, Alfred A., Olav M. Kvalheim, and Rance A. Velapoldi. "Quantitative analysis in diffuse reflectance spectrometry: a modified Kubelka-Munk equation." *Vibrational Spectroscopy* 9, no. 1 (1995): 19-27.
27. Dasineh Khiavi, Negar, Reza Katal, Saeideh Kholghi Eshkalak, Saeid Masudy-Panah, Seeram Ramakrishna, and Hu Jiangyong. "Visible Light Driven Heterojunction Photocatalyst of CuO–Cu_2O Thin Films for Photocatalytic Degradation of Organic Pollutants." *Nanomaterials* 9, no. 7 (2019): 1011.
28. He, Wenjie, Yanjuan Sun, Guangming Jiang, Yuhan Li, Xianming Zhang, Yuxin Zhang, Ying Zhou, and Fan Dong. "Defective Bi_4MoO_9/Bi metal core/shell heterostructure: enhanced visible light photocatalysis and reaction mechanism." *Applied Catalysis B: Environmental* 239

(2018): 619-627.

29. Gao, Xin, Changchang Ma, Wei Ma, Rongru Chen, Yang Liu, Zhi Liu, Zhi Zhu, Pengwei Huo, and Yongsheng Yan. "Novel RGO and concave cube Cu_2O co-modified $BiVO_4$ nanosheets with enhanced photocatalytic and surface adsorption performances of tetracycline." *Nano* 14, no. 02 (2019): 1950015.
30. Mosleh, Soleiman, Mahmood Reza Rahimi, Mehrorang Ghaedi, Kheibar Dashtian, and Shaaker Hajati. "Sonochemical-assisted synthesis of $CuO/Cu_2O/Cu$ nanoparticles as efficient photocatalyst for simultaneous degradation of pollutant dyes in rotating packed bed reactor: LED illumination and central composite design optimization." *Ultrasonics sonochemistry* 40 (2018): 601-610.
31. Dasineh Khiavi, Negar, Reza Katal, Saeideh Kholghi Eshkalak, Saeid Masudy-Panah, Seeram Ramakrishna, and Hu Jiangyong. "Visible Light Driven Heterojunction Photocatalyst of CuO–Cu_2O Thin Films for Photocatalytic Degradation of Organic Pollutants." *Nanomaterials* 9, no. 7 (2019): 1011.
32. Jiang, Denghui, Jianbin Xue, Liqiong Wu, Wei Zhou, Yuegang Zhang, and Xinheng Li. "Photocatalytic performance enhancement of CuO/Cu_2O heterostructures for photodegradation of organic dyes: effects of CuO morphology." *Applied Catalysis B: Environmental* 211 (2017): 199-204.
33. Liang, Ruowen, Shuiguang Luo, Fenfen Jing, Lijuan Shen, Na Qin, and Ling Wu. "A simple strategy for fabrication of Pd@ MIL-100 (Fe) nanocomposite as a visible-light-driven photocatalyst for the treatment of pharmaceuticals and personal care products (PPCPs)." *Applied Catalysis B: Environmental* 176 (2015): 240-248.
34. Kundu, Samapti, Biswarup Satpati, Tanusree Kar, and Swapan Kumar Pradhan. "Microstructure characterization of hydrothermally synthesized $PANI/V_2O_5{\cdot}nH_2O$ heterojunction photocatalyst for visible light induced photodegradation of organic pollutants and non-absorbing colorless molecules." *Journal of hazardous materials* 339 (2017): 161-173.